

# Run 12 Analysis

S. Heppelmann

February 21, 2013

# Contents

<b>I</b>	<b>Setup</b>	<b>3</b>
	Introduction to Run 12 Transverse Spin FMS Analysis . . . . .	4
	List of Runs Used in this Analysis . . . . .	4
	Polarization . . . . .	6
	Data Selection . . . . .	6
<b>II</b>	<b>Transverse <math>A_N</math> of <math>\pi^0</math> at <math>\sqrt{s} = 200</math> GeV</b>	<b>10</b>
	$A_N$ for (200 mRad cone) $\pi^0$ 's. . . . .	11
	$A_N$ for (200 mRad cone) $\pi^0$ 's but with soft energy $< .5$ GeV. . . . .	13
	$A_N$ for (35 mRad cone) $\pi^0$ 's but with soft energy $> .5$ GeV. . . . .	14
	Comparison Between Jet-like $\pi^0$ 's and Isolated $\pi^0$ 's . . . . .	18
	Compare $\pi^0$ $A_N$ to FPD result: 35mR and $E_{soft} < .5$ GeV. . . . .	21
<b>III</b>	<b>Consistency Checks</b>	<b>25</b>
	Consistency of Top FMS and Bottom FMS . . . . .	26
	Yellow Beam Asymmetry . . . . .	28
	Fill Dependent Asymmetry . . . . .	30
<b>IV</b>	<b><math>A_N</math> vs Topology</b>	<b>32</b>
	Compare 3 Photon vs 2 Photon clusters . . . . .	33
	Azimuthal Angular Dependence of Non-Cluster Photons (35mR 2 Photon Cluster) . . . . .	35
	Azimuthal Angular Dependence of $A_N$ for $\pi^0$ Pairs. . . . .	38
	$A_N$ vs Energy Sum of $\pi^0$ Pair. . . . .	43

<b>V</b>	<b><math>A_N</math> vs Transverse Momentum</b>	<b>45</b>
	Compare 200GeV and 500 GeV Dependence on $p_T$ . . . . .	48

# Part I

## Setup

# Introduction to Run 12 Transverse Spin FMS Analysis

In this note I discuss the analysis of part of the Run 12 transverse polarization FMS data. This note describes the transverse momentum and energy dependence of the  $\pi^0$  transverse asymmetry. We also analyze the  $\eta$  meson by determining the signal and background fractions and measuring the asymmetries from the combined signal and background to extract the asymmetry of the  $\eta$ .

## List of Runs Used in this Analysis

This analysis is based on analysis of Run 12 data,  $\sqrt{s} = 200\text{GeV}$  and transverse polarization. The forward asymmetries are measured relative to the blue beam with the FMS so forward asymmetries are based on the polarization in the blue beam.

This analysis is organized by collecting the files into 109 run sets with 627 runs collected between Day 48 and Day 72 of the 2012 proton RHIC run.

The set names and run numbers are listed below.

Set set048z	Runs	13048042	13048043	13048044	13048045	13048048
Set set048y	Runs	13048049	13048050	13048051	13048052	13048053
Set set048x	Runs	13048087	13048088	13048089	13048090	13048091 13048092
Set set049z	Runs	13049004	13049005	13049006	13049031	13049032 13049035 13049039
Set set049y	Runs	13049041	13049042	13049045	13049046	13049047 13049048 13049050
Set set049x	Runs	13049072	13049079	13049080	13049081	13049082
Set set049w	Runs	13049086	13049087	13049088	13049092	13049093
Set set049v	Runs	13049094	13049096	13049098	13049099	13049101
Set set050z	Runs	13050001	13050002			
Set set050y	Runs	13050006	13050007	13050008	13050009	13050010 13050011
Set set050x	Runs	13050012	13050014	13050016	13050020	13050022 13050023
Set set050w	Runs	13050025	13050026	13050027	13050028	13050029 13050031
Set set050v	Runs	13050032	13050033	13050036	13050037	13050038 13050039 13050041
Set set050u	Runs	13050042	13050043	13050044	13050046	13050047 13050049 13050050
Set set051z	Runs	13051006	13051007	13051008	13051009	13051010 13051011
Set set051y	Runs	13051012	13051013	13051014	13051015	13051016 13051017 13051019
Set set051x	Runs	13051020	13051021	13051022	13051023	13051024 13051026 13051028
Set set051w	Runs	13051068	13051069	13051070	13051071	
Set set051v	Runs	13051072	13051073	13051074	13051081	13051082 13051083
Set set051u	Runs	13051084	13051085	13051086	13051087	13051088 13051091
Set set051t	Runs	13051092	13051093	13051095	13051099	13051101
Set set052z	Runs	13052001	13052002	13052003	13052004	13052005 13052008
Set set052y	Runs	13052009	13052010	13052011	13052012	13052013 13052014
Set set052x	Runs	13052015	13052016	13052017	13052018	
Set set052w	Runs	13052036	13052037	13052039	13052042	13052043 13052045 13052046
Set set052v	Runs	13052048	13052049	13052050	13052051	13052052 13052056 13052060
Set set052u	Runs	13052061	13052062	13052064	13052067	13052085 13052087 13052088

Set set053z Runs 13053004 13053005 13053006 13053007 13053010 13053011  
Set set053y Runs 13053012 13053013 13053014 13053015 13053022 13053023  
Set set053x Runs 13053024 13053025 13053026 13053027 13053028 13053029  
Set set054z Runs 13054004 13054005 13054006 13054007 13054008 13054009  
Set set054y Runs 13054010 13054011 13054012 13054013 13054014 13054015  
Set set054x Runs 13054016 13054017 13054018 13054019 13054020 13054021 13054023  
Set set054w Runs 13054042 13054043 13054044 13054047 13054049 13054050  
Set set054v Runs 13054056 13054058 13054060 13054061 13054062 13054063  
Set set054u Runs 13054064 13054065 13054066 13054068 13054069 13054070 13054071  
Set set054t Runs 13054082 13054083 13054084 13054085  
Set set055z Runs 13055001 13055002 13055003 13055004 13055006 13055007 13055008  
Set set055y Runs 13055009 13055010 13055011 13055014 13055015 13055016 13055017  
Set set055x Runs 13055018 13055019 13055020 13055021 13055022 13055023 13055024  
Set set055w Runs 13055034 13055035 13055036 13055037 13055038 13055039  
Set set055v Runs 13055067 13055068 13055069 13055070 13055071 13055072 13055073  
Set set055u Runs 13055075 13055076 13055078 13055079 13055080 13055081 13055082  
Set set055t Runs 13055083 13055085 13055086 13055087 13055088 13055089 13055090  
Set set056u Runs 13056048 13056050  
Set set056z Runs 13056004 13056005 13056007 13056008 13056011 13056012  
Set set056y Runs 13056017 13056020 13056021 13056022 13056023 13056024  
Set set056x Runs 13056025 13056026 13056027 13056028 13056029  
Set set056w Runs 13056030 13056031 13056032 13056033 13056034  
Set set056v Runs 13056035 13056037 13056038 13056039  
Set set057h Runs 13057005 13057006 13057007 13057008 13057009 13057010  
Set set057i Runs 13057011 13057014 13057015 13057016 13057017 13057018 13057019  
Set set057j Runs 13057021 13057022 13057023 13057024 13057025 13057026 13057027 13057038  
Set set057k Runs 13057042 13057043 13057044 13057045 13057046 13057047  
Set set057l Runs 13057048 13057049 13057050 13057051 13057052 13057053  
Set set057m Runs 13057055 13057056 13057057  
Set set058z Runs 13058001 13058002 13058003  
Set set058y Runs 13058007 13058008 13058012 13058013 13058014  
Set set058v Runs 13058015 13058016 13058017 13058018 13058019 13058020  
Set set058x Runs 13058023 13058025 13058026 13058028 13058029 13058031 13058032  
Set set059z Runs 13059002 13059005 13059006 13059007 13059008 13059009  
Set set059y Runs 13059010 13059011 13059012 13059013 13059014  
Set set059x Runs 13059015 13059016 13059017 13059018 13059020  
Set set059w Runs 13059021 13059022 13059023 13059025 13059026 13059027  
Set set059v Runs 13059033 13059035 13059037 13059038 13059039  
Set set059u Runs 13059074 13059076 13059077 13059078 13059079 13059080 13059082  
Set set059t Runs 13059083 13059084 13059085 13059086 13059087 13059089  
Set set060z Runs 13060001 13060002 13060003  
Set set060y Runs 13060005 13060007 13060008 13060009 13060010 13060011 13060012  
Set set061z Runs 13061017 13061019 13061024 13061025  
Set set061y Runs 13061029 13061030 13061031 13061035  
Set set061x Runs 13061053 13061054 13061055 13061056 13061059  
Set set062z Runs 13062001 13062002 13062004  
Set set062y Runs 13062005 13062006 13062007  
Set set062x Runs 13062013 13062014  
Set set062w Runs 13062023 13062025 13062026 13062027 13062028 13062029  
Set set062v Runs 13062031 13062036 13062042 13062044 13062045 13062046  
Set set062u Runs 13062047 13062049 13062050 13062053 13062057  
Set set062t Runs 13062059 13062061 13062062 13062063  
  
Set set063z Runs 13063006 13063008 13063009 13063010 13063011 13063012  
Set set063y Runs 13063017 13063019 13063020 13063022 13063023 13063025  
Set set063x Runs 13063029 13063030 13063031 13063032 13063034 13063035 13063036  
Set set063w Runs 13063051 13063052 13063053 13063054 13063059 13063060 13063061

```

Set set063v Runs 13063062 13063063 13063064 13063065 13063067 13063068
Set set063u Runs 13063070 13063071 13063072 13063073 13063074 13063076
Set set064z Runs 13064001 13064002 13064003 13064004 13064005 13064006
Set set064y Runs 13064009 13064012 13064014 13064020 13064021 13064022
Set set064x Runs 13064023 13064024 13064025 13064026 13064027 13064028
Set set064w Runs 13064029 13064031 13064032
Set set065z Runs 13065004 13065012 13065025
Set set065y Runs 13065048 13065049 13065050 13065052 13065053 13065055
Set set065x Runs 13065056 13065058 13065059 13065060
Set set066w Runs 13066004 13066009 13066012 13066015 13066019 13066021
Set set066v Runs 13066022 13066023 13066024 13066025 13066026 13066027 13066028
Set set066u Runs 13066029 13066030 13066031 13066033 13066034 13066035 13066036
Set set068z Runs 13068057 13068058 13068059 13068060 13068084 13068085
Set set068y Runs 13068086 13068087 13068090
Set set069z Runs 13069001 13069002 13069003 13069004 13069005 13069006 13069007 13069008
Set set069y Runs 13069013 13069014 13069016 13069017 13069018 13069020
Set set069x Runs 13069021 13069022 13069023 13069024 13069026 13069027
Set set069w Runs 13069030 13069031 13069035
Set set070z Runs 13070017 13070018 13070020 13070021 13070022 13070024
Set set070y Runs 13070025 13070026 13070027 13070050 13070051 13070052
Set set070x Runs 13070054 13070056 13070058 13070059 13070065
Set set071z Runs 13071003 13071004 13071005 13071008 13071009 13071010 13071011 13071012
Set set071y Runs 13071028 13071029 13071031 13071032 13071033 13071035
Set set071x Runs 13071041 13071042 13071043 13071045 13071046 13071048
Set set071w Runs 13071049 13071050 13071051 13071054 13071055
Set set071v Runs 13071064
Set set072z Runs 13072001 13072002 13072003 13072004 13072005 13072006
Set set072y Runs 13072007 13072008 13072009 13072010 13072011 13072014
Set set072x Runs 13072015 13072016 13072017 13072018 13072019 13072020

```

## Polarization

For this analysis, the assumption  $P_{blue}=60\%$  is used for all analysis of forward  $A_N$  with the polarized blue beam.

## Data Selection

For this analysis the clusters of photon candidates are collected from all parts of the FMS.

- The basic reconstruction involves identifying "**real**" hit clusters as candidates for photons. The selection of real hit clusters are restricted to **hit-cluster energy > 2.0 GeV** in the small cell region of the FMS and **hit-cluster energy > 0.75 GeV** for the large cell region. Note: most isolated minimum ionizing hadrons have energy less than 1 GeV and will be thus ignored at the first stage of photon reconstruction and thus from all subsequent analysis.

- A list of photon candidates is generated from the hit cluster list, for events that pass the jet trigger. Photon candidates must come from "real" hit clusters and photons must have energies greater than 6 GeV. Photon candidates with energy less than 6 GeV (soft photons) are ignored in the construction of the hard photon list. It is the hard photon list that we use to select mesons for this analysis, however the real clusters with energy less than 6 GeV can contribute to a soft energy sum.
- We divide the photon lists into photon clusters. We will build  $\pi^0$ 's or other mesons from photons within a particular photon cluster. The definition of a photon cluster is given by a clustering algorithm. Photon candidates are sorted by energy, starting with the highest energy photon first. The highest energy is the seed of the first cluster. We add photons to existing clusters if they are within an angular cone of the cluster momentum direction as defined before the new photon is added. Photons are tested for inclusion in the order from highest momentum to lower momentum. After a cluster is completed, the remaining unused photons are used to make additional clusters.
- A new cluster is created when a photon is encountered but no pre-existing cluster is found within an angle  $\Delta\theta$  from the new cluster location.
- As photons are added to clusters, the cluster direction is recalculated.
- Around each cluster, we sum the soft energy that is found within a "jet like cone" of  $\Delta\eta_{soft}$  and  $\Delta\phi_{soft}$  from the cluster axis.

This analysis was based on clusters created with the angle  $\Delta\theta = 200mR$  and  $\Delta\theta = 35mR$ . In addition, when we discuss the soft energy contribution to a cluster, will sum the soft energy within a cone of  $\sqrt{\Delta\eta^2 + \Delta\phi^2} < 0.9$  from the cluster direction. The same soft energy can contribute to more than one cluster.

For 2 photon clusters collected with the  $\Delta\theta = 200mR$  selection cone, the average soft energy is about 2. GeV. Between 1/2 of the two photon clusters have less than 0.5 GeV of soft background energy. Remember that soft energy contributions come from real photon clusters so the minimum non-zero soft energy will be .75 GeV or 2 GeV depending whether the energy is deposited in the large or small cells.



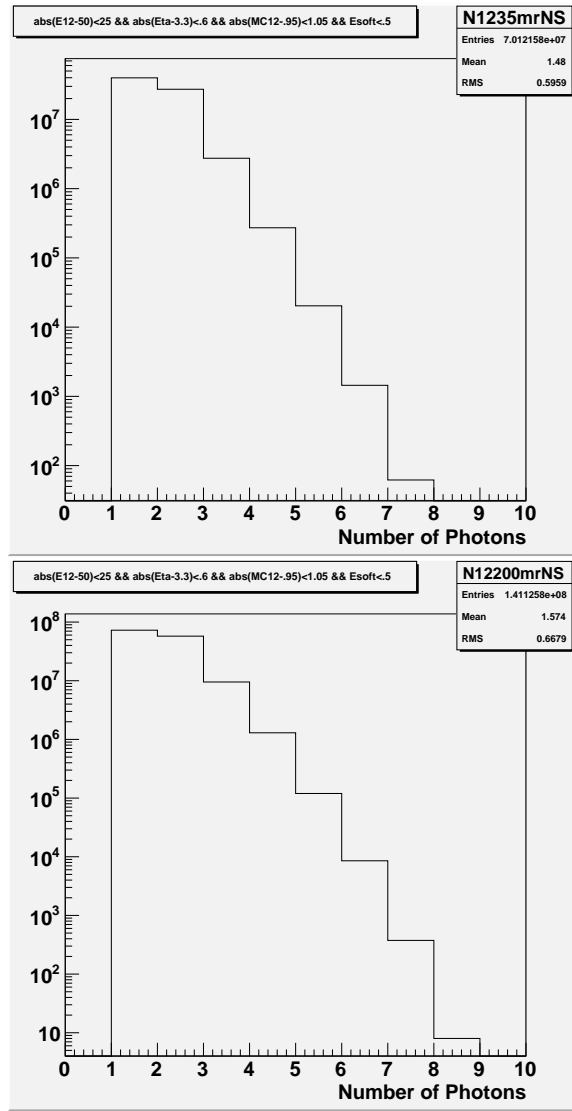


Figure 1: The distribution of the number of photons in a cluster is shown for isolated clusters of photons selected, in the top frame with a 35 mR cluster cone and in the bottom frame with a 200mR cluster cone. Selected events have also have less than 0.5 Gev of soft energy in a 0.9 radian jet cone. All clusters have cluster energy:  $25 \text{ GeV}/c < \text{Energy} < 75 \text{ GeV}$ , cluster mass less than  $2 \text{ GeV}$  and  $Z < .5$ . With 142 million such clusters (with  $\Delta\theta = 200mR$ ), the number of 2 photon clusters is about 57 million, with about 71 million 1 photon clusters. There are about million 9 photon clusters that pass the above selection test. For the 35 mR cone selection, the numbers are 40/27/3 million for the 1/2/3 photon cluster event counts.

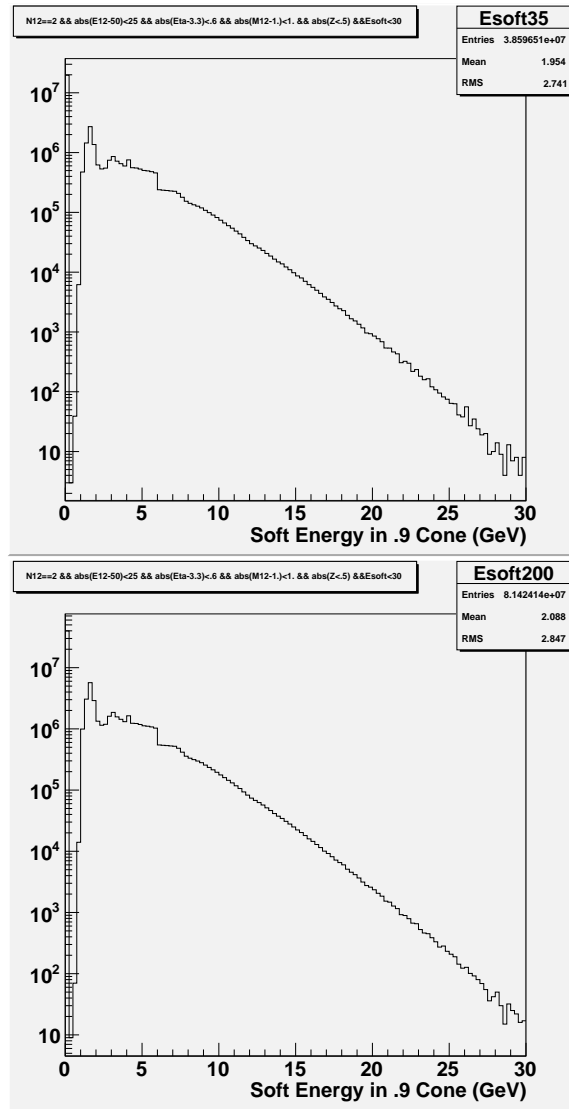


Figure 2: The distribution of soft energy near a cluster is shown for isolated clusters of photons selected with a 35 mR cone (top frame) and a 200 mR cone (bottom frame). All clusters in this plot have 2 photons with cluster energy:  $25 \text{ GeV} < \text{Energy} < 75 \text{ GeV}$ , cluster mass less than  $2 \text{ GeV}$ . The energy distribution shown is the sum of soft energy within a 0.9 radian jet cone about the 2 photon core.

## Part II

Transverse  $A_N$  of  $\pi^0$  at  
 $\sqrt{s} = 200 \text{ GeV}$

## $A_N$ for (200 mRad cone) $\pi^0$ 's.

The analysis presented in this section is based on selection of photon clusters using a cone radius ( $\Delta\theta < 200mR$ ). The soft energy is ignored in this analysis. Events were selected as  $\pi^0$ 's if the mass was less than 0.4 GeV.

This is a large cone radius; only about 20% of the events with 2 photon clusters of this size also have additional photons outside the cluster. For the 20% with away side photons, the average away side energy is about 14 GeV.

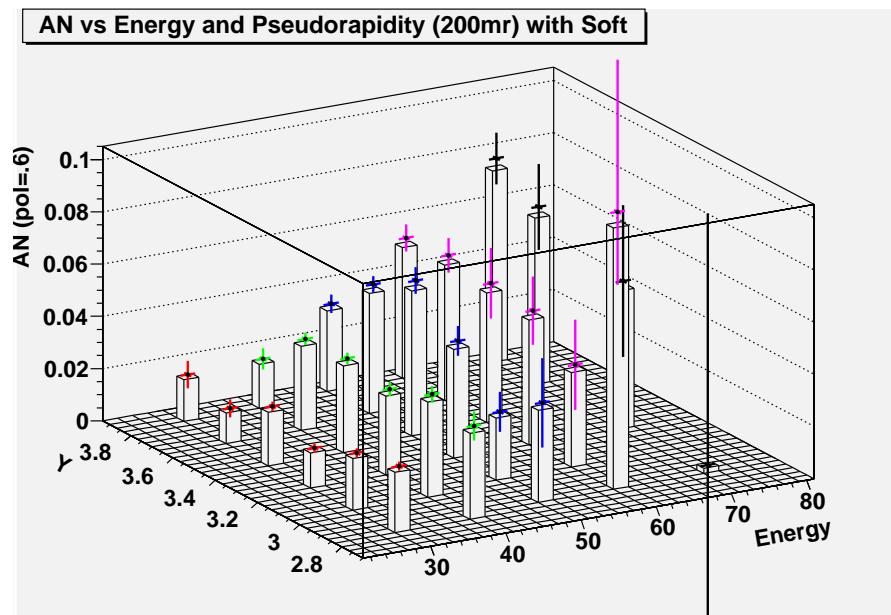


Figure 3: The dependence of  $A_N$  on Energy and Pseudorapidity **for isolated clusters of photons selected with a 200 mR cone**. Soft energy in (0.9 radian jet cone) is ignored in these plots.

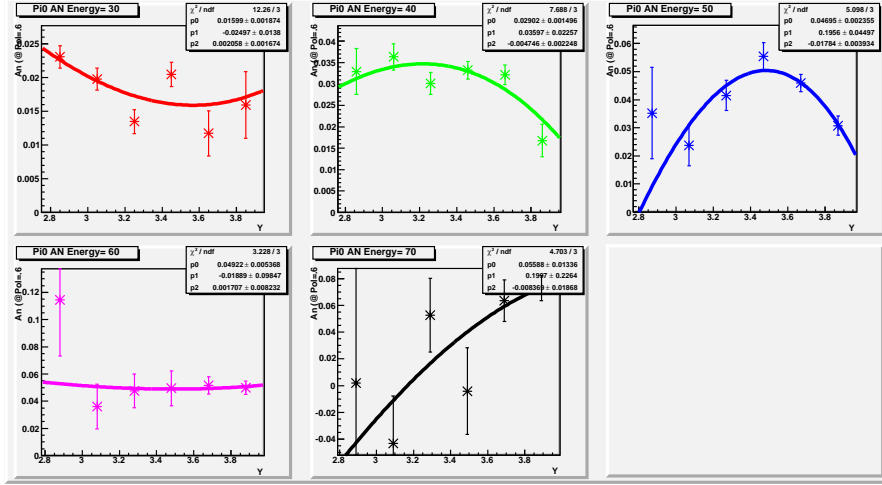


Figure 4: The dependence of  $A_N$  of  $\pi^0$ 's on Energy and Pseudorapidity for 2 photon isolated clusters selected with a 200 mR cone. Soft energy (0.9 radian jet cone) is ignored in these plots.

The essential features of these plots is that for large at small  $x_F$ , ( see 30 GeV energy bin,  $0.25 < x_F < .35$ ) we observe a decrease in asymmetry as pseudo-rapidity increases from 2.85 to 3.85. **The asymmetry clearly rises with  $p_T$  out to our limit (corresponding to  $p_T \simeq 4.5 GeV/c$ ) for this energy range.**

This trend may reverse at larger energy, ( $x_F \geq .5$ ), with a maximum in  $A_N$  emerging at about  $Y = 3.4$  and a falling asymmetry for larger  $p_T$ .

The selection of 2 photon clusters with such a large cone tends to select simple events without other significant jet components. However, if we do observe soft underlying energy in a typical jet cone, that would be evidence for  $\pi^0$ 's from jet fragmentation. The results shown in Figure 4 contains events both with and without associated soft energy within the jet cone of cone radius 0.9.

## $A_N$ for (200 mRad cone) $\pi^0$ 's but with soft energy $< .5\text{GeV}$ .

This analysis differs from that of the previous section only by the requirement of  $E_{soft} < 9.5 \text{ GeV}$  within the jet cone radius of 0.9. This makes the  $\pi^0$  more isolated and less jet like that those analyzed in the previous section.

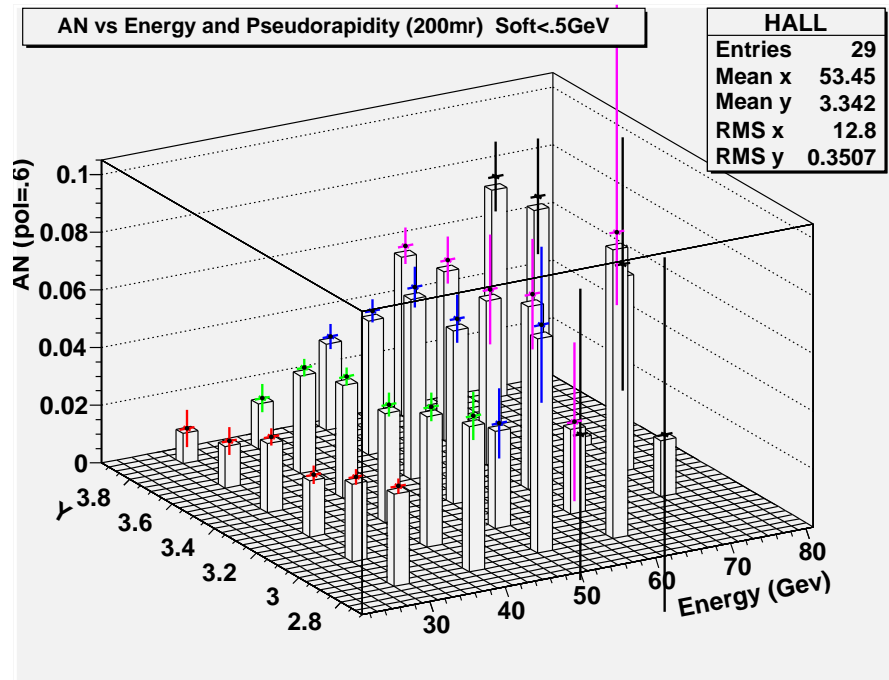


Figure 5: The dependence of  $A_N$  of  $\pi^0$ 's on Energy and Pseudorapidity for 2 photon isolated clusters, selected with a 200 mR cone. Soft energy is (0.9 radian jet cone) less than 0.5 GeV in these plots.

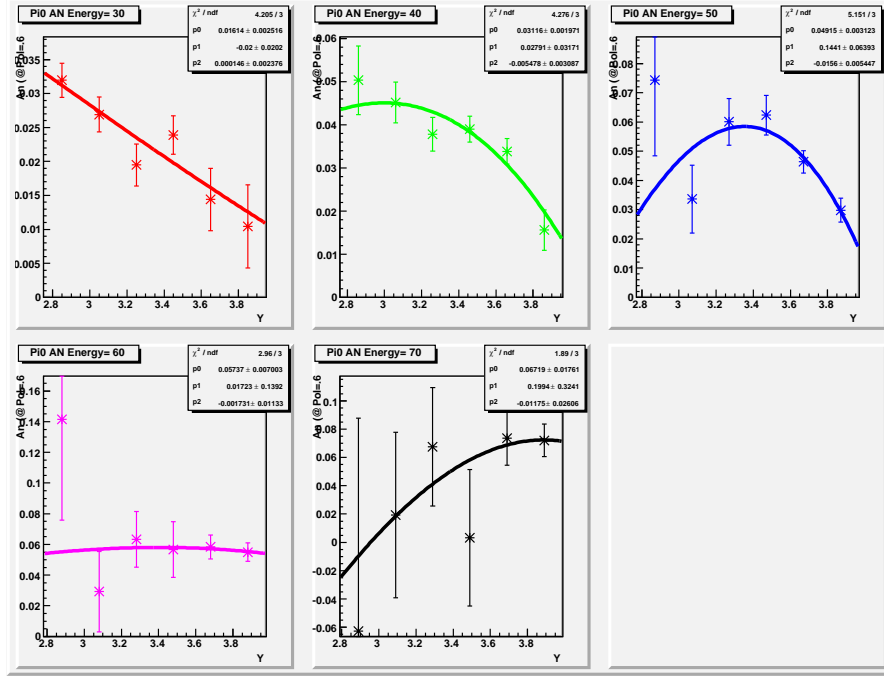


Figure 6: The dependence of  $A_N$  on Energy and Pseudorapidity **for isolated clusters of photons selected with a 200 mR cone**. Soft energy (in 0.9 radian jet cone) less than 0.5 GeV in these plots.

The stronger isolation cuts used to make Figure 6, as compared to the more jet-like  $\pi^0$  environment for the cuts used in Figure 4, leads to more severe increase of  $A_N$  with  $p_T$  at lower energies ( $0.25 < x_F < 0.45$ ). The larger energy ( $0.45 < x_F < .75$ ) behavior may be similar in the two figures.

The conclusion may be that the dramatic increase in  $A_N$  with  $p_T$ , at lower values of  $X_F$ , may arise from a non-jet like component of  $\pi^0$  production. From a component that is more exclusive in nature than inclusive.

**$A_N$  for (35 mRad cone)  $\pi^0$ 's but with soft energy  $> .5\text{GeV}$ .**

The most jet-like selection of  $\pi^0$ 's would involve selection of a pair of photons in the smallest possible cone, with the requirement of soft energy in the

vicinity of the  $\pi^0$ . To select for this, we will consider 2 photons in a cluster of angular size ( $\Delta\theta < 35mR$ ). We will also demand that events have soft energy within  $\sqrt{\Delta\eta^2 + \Delta\phi^2} < 0.9$ . This is complementary to the selection described in the last section, which was maximally isolated. This analysis is for  $\pi^0$ 's correlated with soft background energy.

Figures 7 and 8 represent the asymmetries from events with  $\pi^0$  that are more likely to be from jet events.



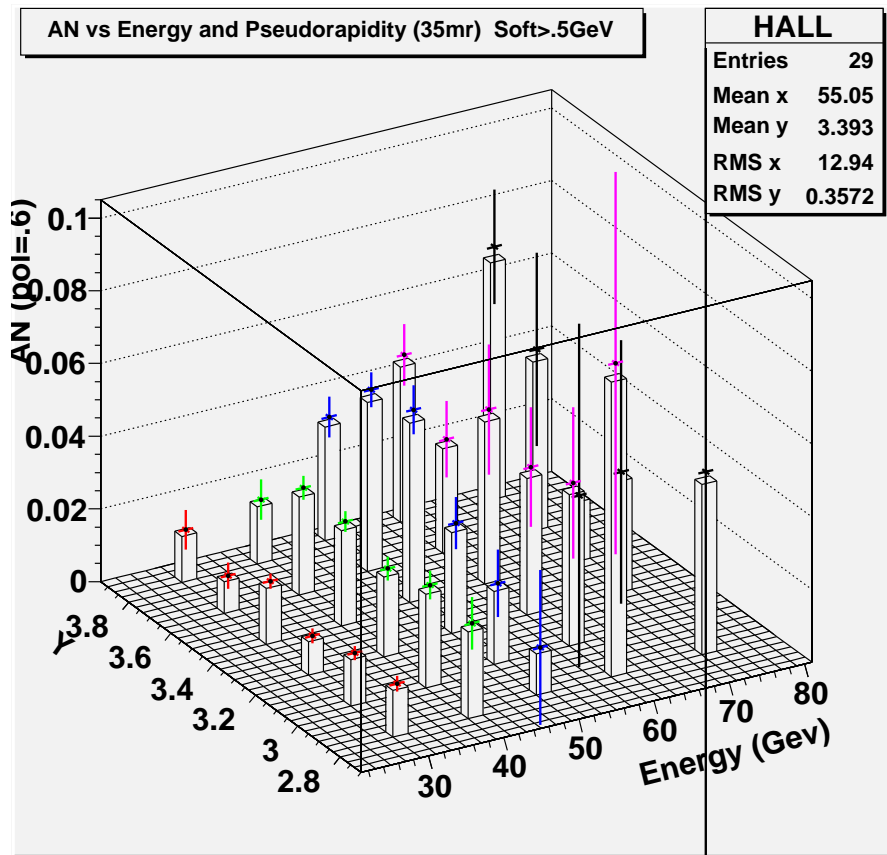


Figure 7: The dependence of  $A_N$  on Energy and Pseudorapidity for clusters of photons selected with a 35 mR cone with soft energy required. Soft energy (in 0.9 radian jet cone) must be greater than 0.5 GeV for events contributing to these plots.

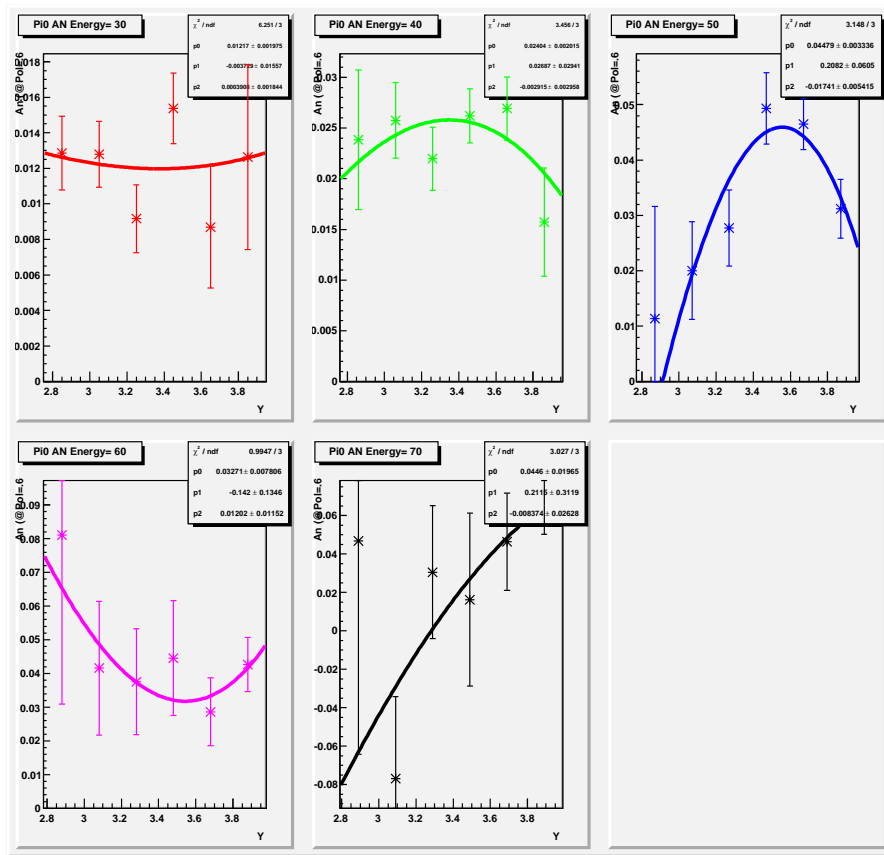


Figure 8: The dependence of  $A_N$  on Energy and Pseudorapidity for two photon events selected with a 35 mR cone. Soft energy in (0.9 radian jet cone) is greater than 0.5 GeV in these plots.

## Comparison Between Jet-like $\pi^0$ 's and Isolated $\pi^0$ 's

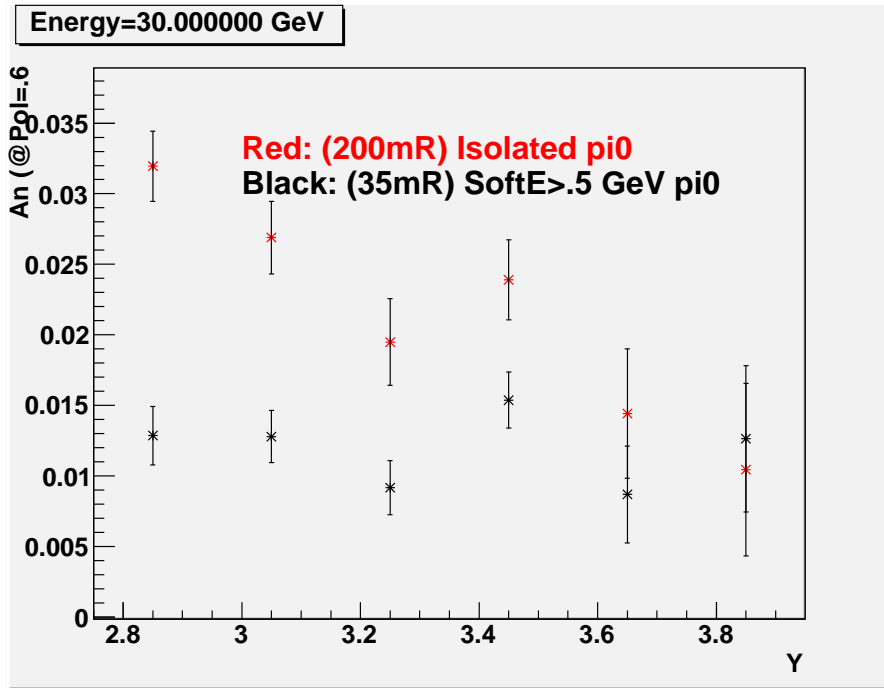


Figure 9: Compare the asymmetries for 30 GeV  $\pi^0$ 's from figure 8 and figure 5. This corresponds to a range of Feynman  $x_F$  ( $0.25 < x_F < 0.35$ ). The red points correspond to the more isolated  $\pi^0$  events and the black points correspond to the more jet-like  $\pi^0$  events. The lowest pseudo-rapidity bins correspond to  $p_T$  in the 4 to 5 GeV/c range. It appears that at low  $p_T$  the asymmetry depends little the soft energy cut but at high  $p_T$  the more jet-like events have smaller values of  $A_N$ , with asymmetry between 1/2 and 1/3 the size of that seen in more isolated  $\pi^0$  events.

We see that in the low  $x_F$  region, the asymmetries are very different for events that contain  $\pi^0$ 's which are likely to come from jet-like events and those that appear to be produced in isolation.

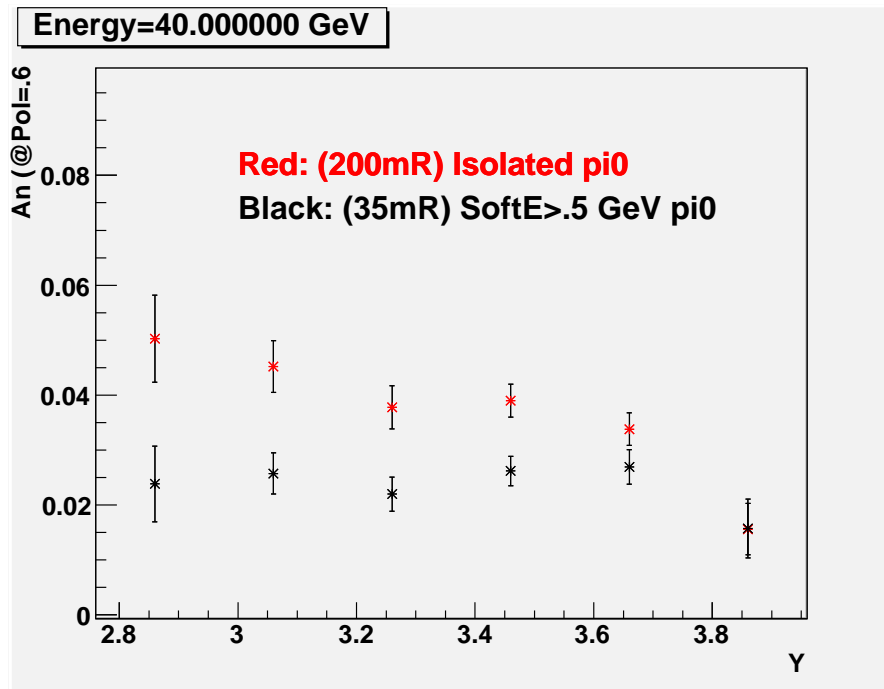


Figure 10: Compare the 40 GeV Asymmetry from figure 8 and figure 5.

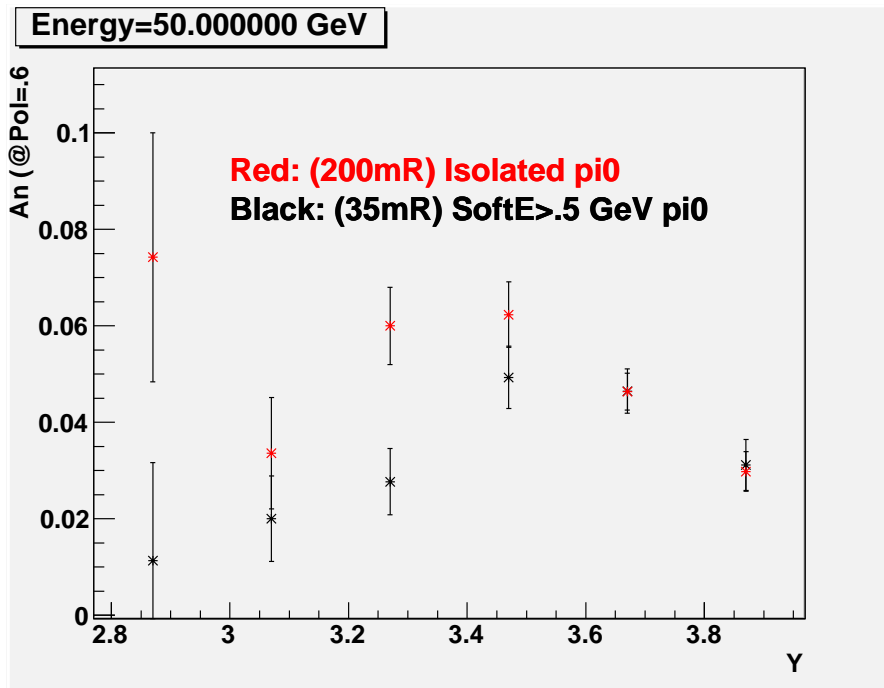


Figure 11: Compare the 50 GeV Asymmetry from figure 8 and figure 5.

It is clear that a jet which fragments to a large  $Z \pi^0$  will tend to produce soft particles around the leading  $\pi^0$ . In the EM calorimeter, many of these soft particles are detected but not all. When we select isolated  $\pi^0$ 's from the point of view of EM energy, we still will include a component of jet-like  $\pi^0$ 's with unobserved soft components.

We see in Figure 9, Figure 10 and Figure 11 that the rise in  $A_N$  with transverse momentum comes mostly from the contribution of isolated  $\pi^0$  production, not from the jet-like production.

We also see that for larger Feynman  $x_F$ ,  $x_F > .5$  (or  $E > 50 \text{ GeV}$ ), the asymmetry may fall with  $p_T$  above  $p_T \simeq 3 \text{ GeV}$ . For jet-like production of  $\pi^0$ 's, the asymmetry may also fall with  $p_T$  at the largest  $p_T$  seen in the FMS.

## Compare $\pi^0$ $A_N$ to FPD result: 35mR and $E_{soft} < .5GeV$ .

To compare this result with the published FPD results, we will consider a data selection that most closely resembles the earlier conditions. The FPD is a 7x7 array with angular size of about 35mR x 35mR. The trigger was based on a threshold for deposited energy in the 49 cell array. The signal was for 2 photon events within the FPD of energy greater than the trigger threshold.

The FMS results should be comparable to the FPD results if we select the photon clusters For (35 mRad cone) but with soft energy  $< .5GeV$ . In Figure 12 we show the dependence of  $A_N$  on energy and pseudo-rapidity for these examples.

In Figure 12, the comparison is between Run 6 published results and new Run 12 data selected with a wide mass cut.

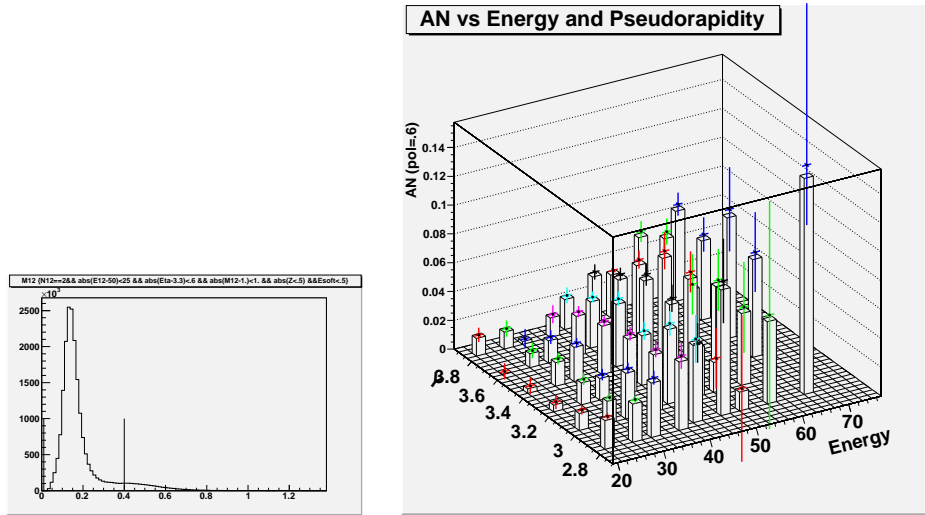


Figure 12: Run 12 event selection includes a mass cut  $0 < mass < 0.4GeV$ . Other selection criteria are defined to be similar to Run 6 FPD selection. The Figure on the right shows the dependence of  $A_N$  on energy and pseudo-rapidity for 2 photon events in 35mR clusters with no observed soft energy ( $E_{soft} < 0.5GeV$ ).

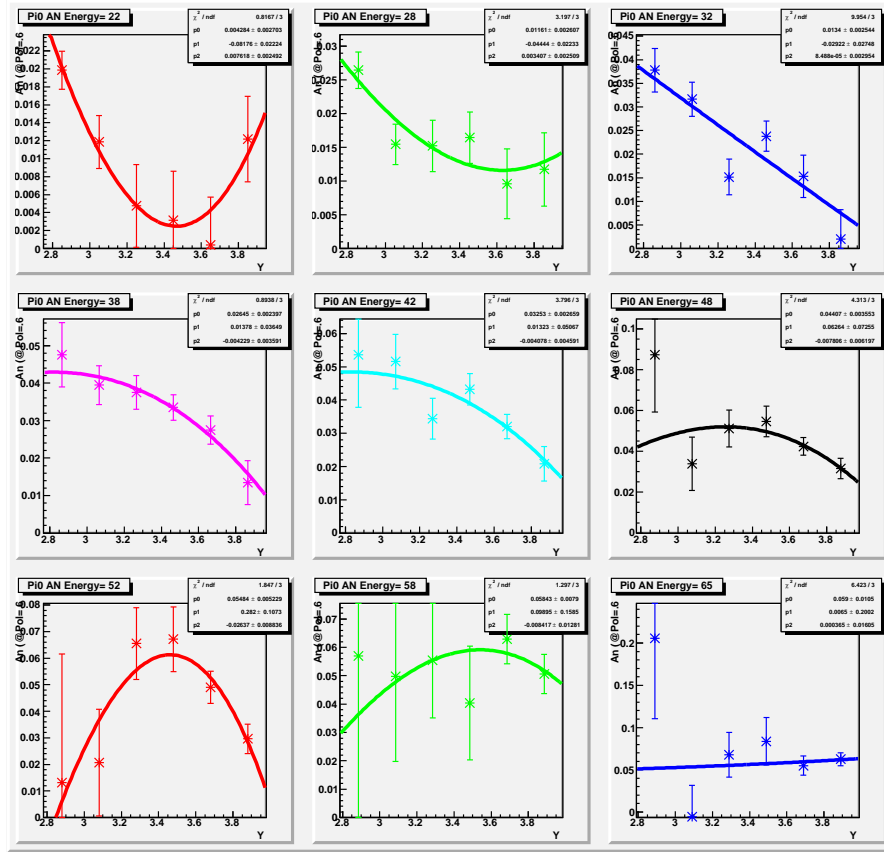


Figure 13: Run 12 event selection includes a mass cut  $0 < mass < 0.4 GeV$  and the same other selection as used for Figure 12. This shows the dependence of  $A_N$  on energy and pseudorapidity for 2 photon events in 35mR clusters with no observed soft energy ( $E_{soft} < 0.5 GeV$ ). Each frame is for the energy indicated. The curves through the points are from a 2nd order polynomial fit.

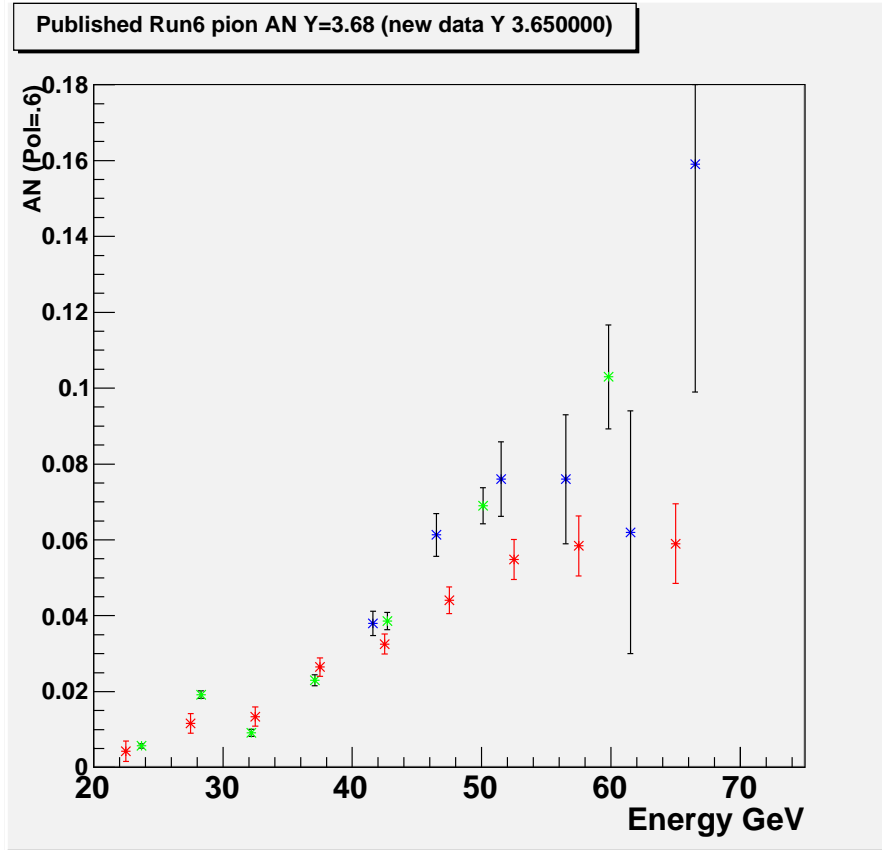


Figure 14: FMS Run 12 data shown with red points. The red point asymmetries and errors are determined from the "pol2" fit shown in Figure 13, evaluated at pseudorapidity of 3.65. Run 12 event selection includes a mass cut  $0 < mass < 0.4 GeV$  and the same other selection as used for Figure 12, with 2 photon events in 35mR clusters with no observed soft energy ( $E_{soft} < 0.5 GeV$ ). The green points are from the Run 6 publication and the center-cut analysis is shown in blue.

At this time, there has been no attempt to remove background under the  $\pi^0$  peak. We expect backgrounds to be less than or equal to 10% of the signal. We know that the asymmetry of the low mass background is much less than the asymmetry of the  $\pi^0$  itself. By reducing the width of the mass cut, we reduce the contribution of background. The width of the mass cut for data in Figure 15 is about half as large as it was in Figure 14. We show



the comparison between the energy dependence of  $A_N$  for Run 6 and for Run 12 where the Run 12 data was selected with the narrow mass cut. With the reduced mass width, the signal to background ratio may be greater than 20. The remaining background correction has not been applied to the Run 12 data points shown in Figure 15. .

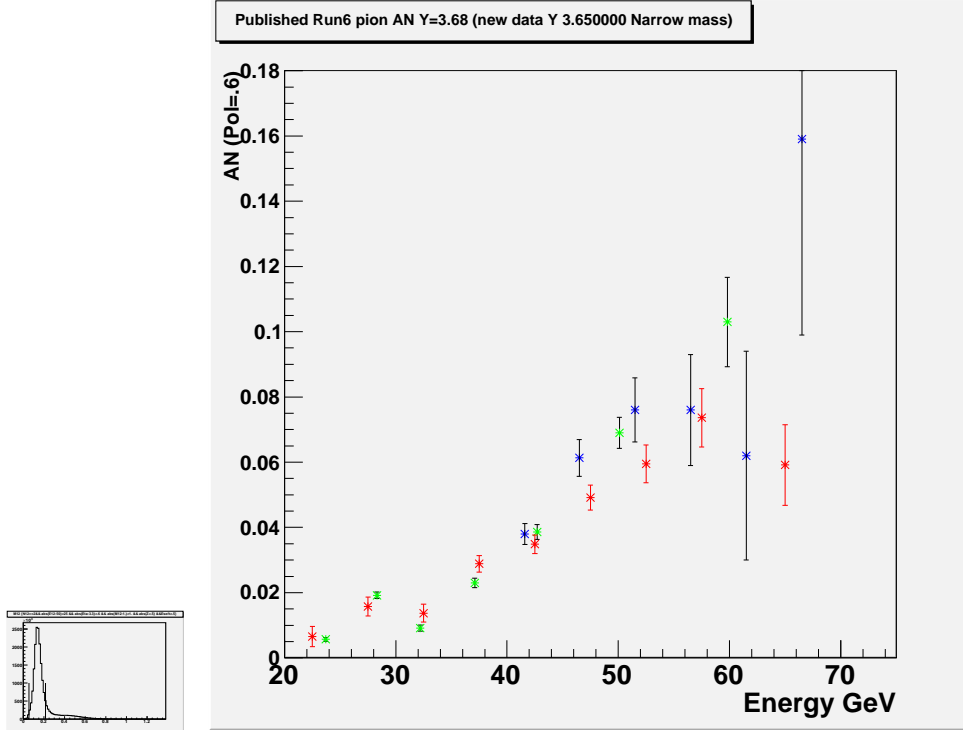


Figure 15: FMS Run 12 data shown with red points. Run 12 event selection includes a mass cut  $.055 < mass < 0.215 GeV$  (as shown in the top figure) and the same other selection as used for Figure 12 with 2 photon events in 35mR clusters with no observed soft energy ( $E_{soft} < 0.5 GeV$ ). The green points are from the Run 6 publication and the center-cut analysis is shown in blue.

The difference between the wide mass cut comparison (Fig 14) and the narrow mass comparison 15 represents the effects of non  $\pi^0$  background.

# Part III

## Consistency Checks

## Consistency of Top FMS and Bottom FMS

We divide the FMS into an upper detector and a lower detector by dividing along the horizontal axis at the beam height. This allows us to make two fairly independent measurements of  $A_N$  using the two partial detectors. It is known that the part of the FMS below the horizontal axis had more problems with magnetic field related inefficiency than did the upper half detector.

The point of this section is to repeat the measurement of the asymmetry with the upper and lower detector and compare the results.

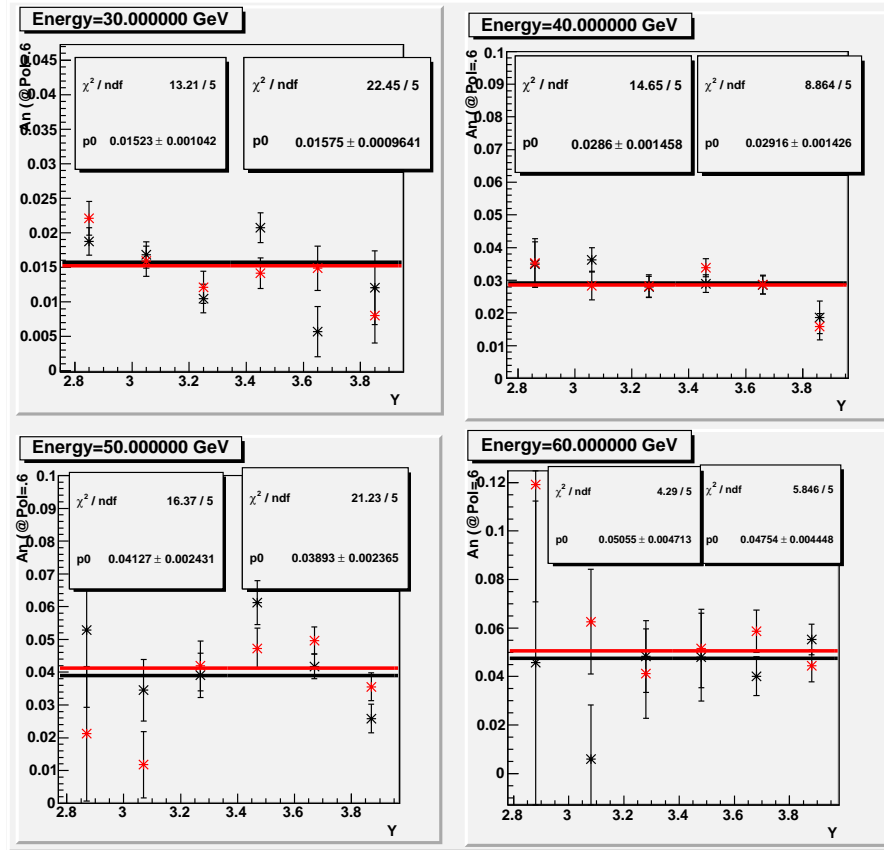


Figure 16: The four frames of this figure represent measurements at 4 energies, 30 GeV, 40 GeV, 50 GeV and 60 GeV. The full width of the energy bins is 10 GeV. The black data points represent the measurement from the lower half of the FMS and the red points are the measurement with the upper half detector. The fits to a constant  $A_N$ , are shown by straight lines. The fit information for the red points is shown in the upper left box for each frame. The upper right box provides fit information for the black points.

We see from Figure 16 that the average  $A_N$  from the upper detector (red points) tend to be somewhat larger than determined from the lower detector (black points). The averages from the upper detector are a few percent larger than the lower detector (up to 5%). However, the difference may not be statistically significant. There is not a large (significant) difference between the measurement made with the upper vs lower half of the FMS

detector. These events were selected to have two tracks in a 35 mR cluster. The additional cuts are  $Z < .5$  and soft energy is ignored.

## Yellow Beam Asymmetry

We measure the transverse asymmetry with this same data with respect to the yellow beam. This, of course, is the asymmetry for backward rapidity. The FMS is forward with respect to the blue beam and backward with respect to the yellow beam.

From Figure 18 we see that the backward Asymmetry is consistent with zero. In particular, for the yellow beam the average asymmetry is

$$\langle A_N \rangle = 9.4 \times 10^{-4} \pm 7.0 \times 10^{-4}$$

Based on the distribution of  $\chi^2$ , these fits to a constant  $A_N$  at each energy, independent of pseudorapidity is not excluded.

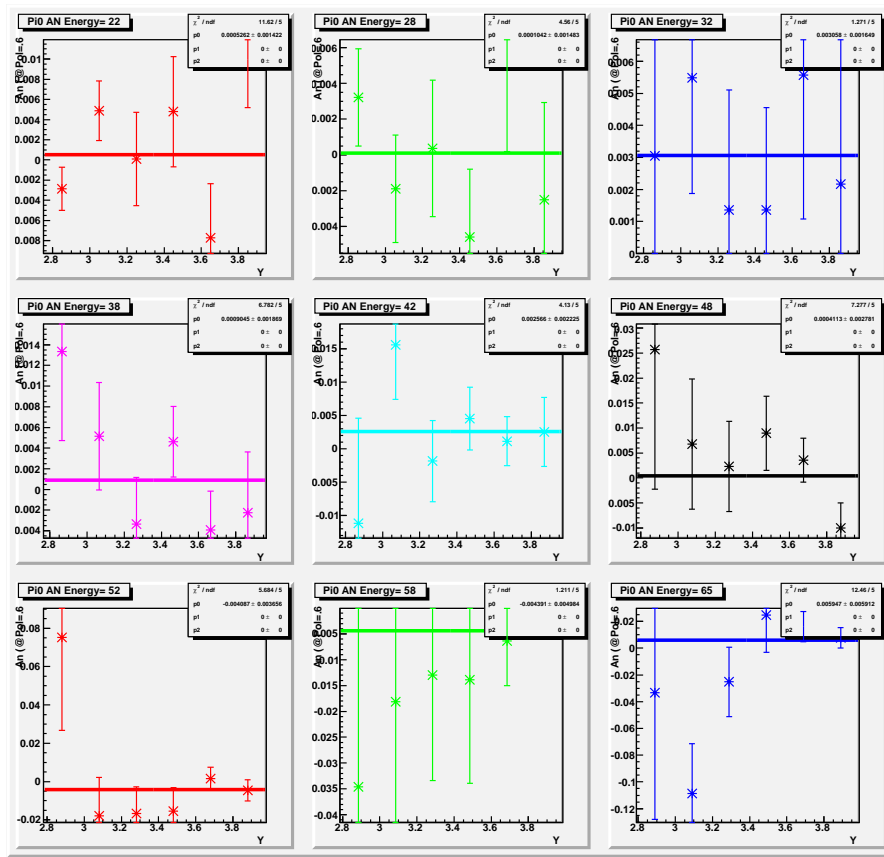


Figure 17: The nine frames of this figure represents the asymmetry as measured relative to the **yellow beam** for the nine energy regions indicated. Each frame shows a fit to a constant. The  $\chi^2$  for nine 1 parameter fits is 54/(45 DOF). There is about a 15% probability that the  $\chi^2$  will be as large as 54 if the fit model is meaningful. The summaries of the fits at each of these average fitted asymmetries at nine energies were shown in Figure 18. These asymmetries are calculated with the assumption that the yellow beam polarization is 60%.

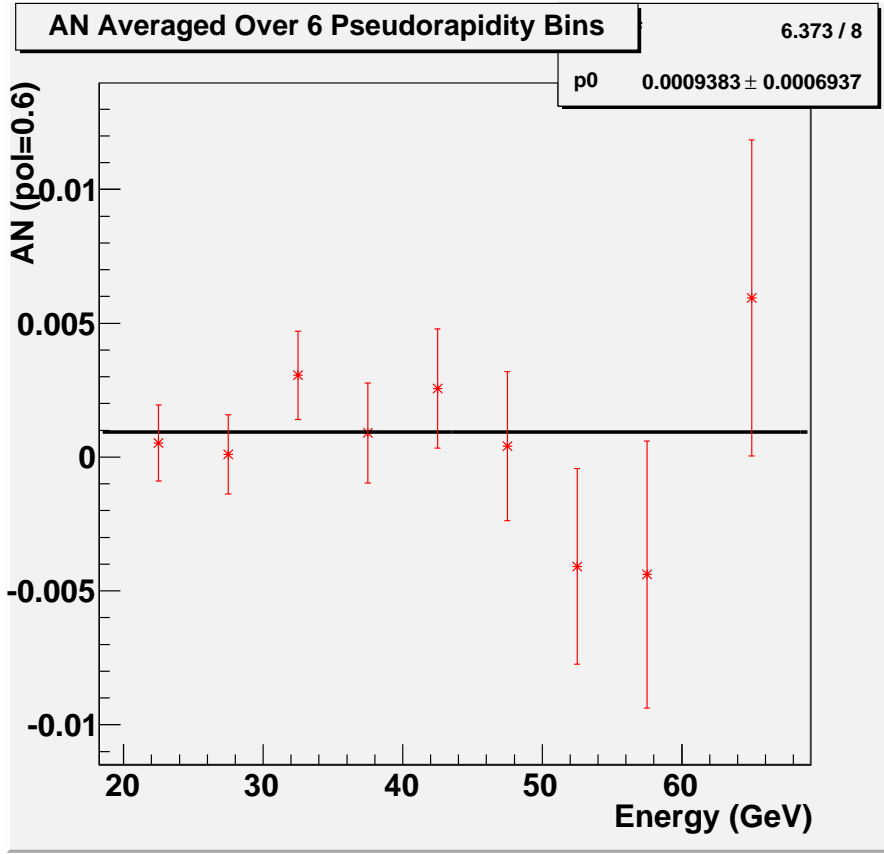


Figure 18: This plot shows the average **yellow beam** asymmetries at each of nine energy regions (see Figure 17). The fitted average of these values of  $A_N$  is indicated. The average yellow beam transverse asymmetry is seen to be  $\langle A_N \rangle = 9.4 \times 10^{-4} \pm 7.0 \times 10^{-4}$ . This is of course consistent with zero.

## Fill Dependent Asymmetry

If we select events (35mR cluster algorithm ) with wide cuts we can measure the transverse asymmetry  $A_N$  on a fill by fill basis.

The  $\chi^2/DOF$  for the constant fit ( $A_N$  independent of fill number) can be taken from Figure 19 both for yellow beam and blue beams. The observed yellow beam asymmetry is nominally zero ( $\langle A_N \rangle = 7 \times 10^{-4} \pm 5 \times 10^{-4}$ ). These variations are greater than expected from random variations. The probability to observe  $\chi^2$  as large as the  $\chi^2 = 62.8$  seen in Figure 19 here for 41 degrees of freedom is less than 2%. The larger  $\chi^2$  could correspond to average fill dependent variation at the level of about  $\sqrt{\langle (\Delta A_N)^2 \rangle} = .002$ .

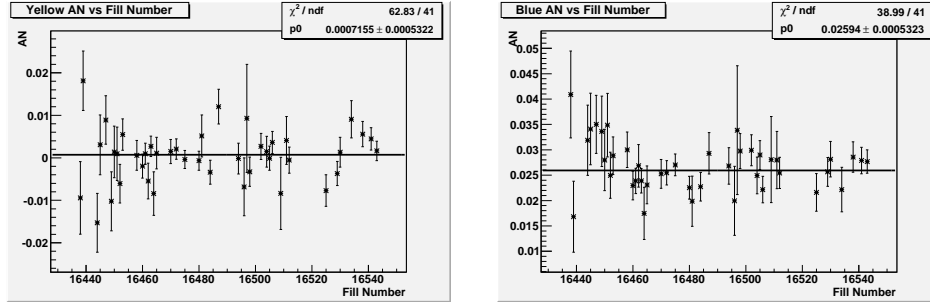
For the blue beam, the variation of blue  $A_N$  is consistent with statistical variations with  $\chi^2/DOF = 40/41$ . It should be noted that the fill by fill vari-

Table 1: The cuts used to define events in Figure 19.

cuts
2 Tracks
$20 \text{ GeV} < \text{Energy} < 80 \text{ GeV}$
$2.7 < \text{pseudorapidity} < 3.9$
$0.035 \text{ GeV} < \text{Mass} < .235 \text{ GeV}$

ations in blue polarization have not been included and will have contributed to the  $\chi^2$  for the assumption of a constant blue asymmetry.

Figure 19: The asymmetry for cuts defined in Table 1. This plot shows the asymmetry vs. fill number (Top:Yellow beam; Bottom:Blue beam) for events defined over a wide range of energy and pseudorapidity. The fits are to a constant value of  $A_N$  independent of Fill number. The plotted asymmetries assume a constant beam polarization of 55%.





## Part IV

### $A_N$ vs Topology

In this section, we continue to explore how the event  $A_N$  asymmetry depends on the event topology. The asymmetry was seen to be associated with events with  $\pi^0$ s found in isolation. To further explore this, we will compare three categories of  $p_0$  events.

## Compare 3 Photon vs 2 Photon clusters

Working with the 35mR cone for collecting photons into clusters, we can select the  $\pi^0$  signal in 3 photon clusters. We will apply the  $\pi^0$  mass cut,  $abs(M12 - .135) < .08$  where  $M12$  is the mass of the highest energy pair of photons. The asymmetries thus obtained are then compared with both the 200mR isolated  $\pi^0$  signal and the 35mR signal with soft energy. The data in Figure 20 is of three types.

- The red squares indicate  $A_N$  for large cluster cone of size 200mR angle and exactly 2 photons in cone with no soft energy.
- The green triangles correspond to small cluster cone of size 35mR angle and exactly 2 photons but with soft energy found (soft energy  $> 0.5$  GeV).
- The blue circles correspond to selection with a cluster cone of size 35mR with exactly 3 photons in the cone, with the two high energy photons of the three forming a  $\pi^0$  mass,  $abs(M12 - .135) < .08$ .  $A_N$  is plotted as a function of the cluster pseudorapidity and the 2 photon energy.

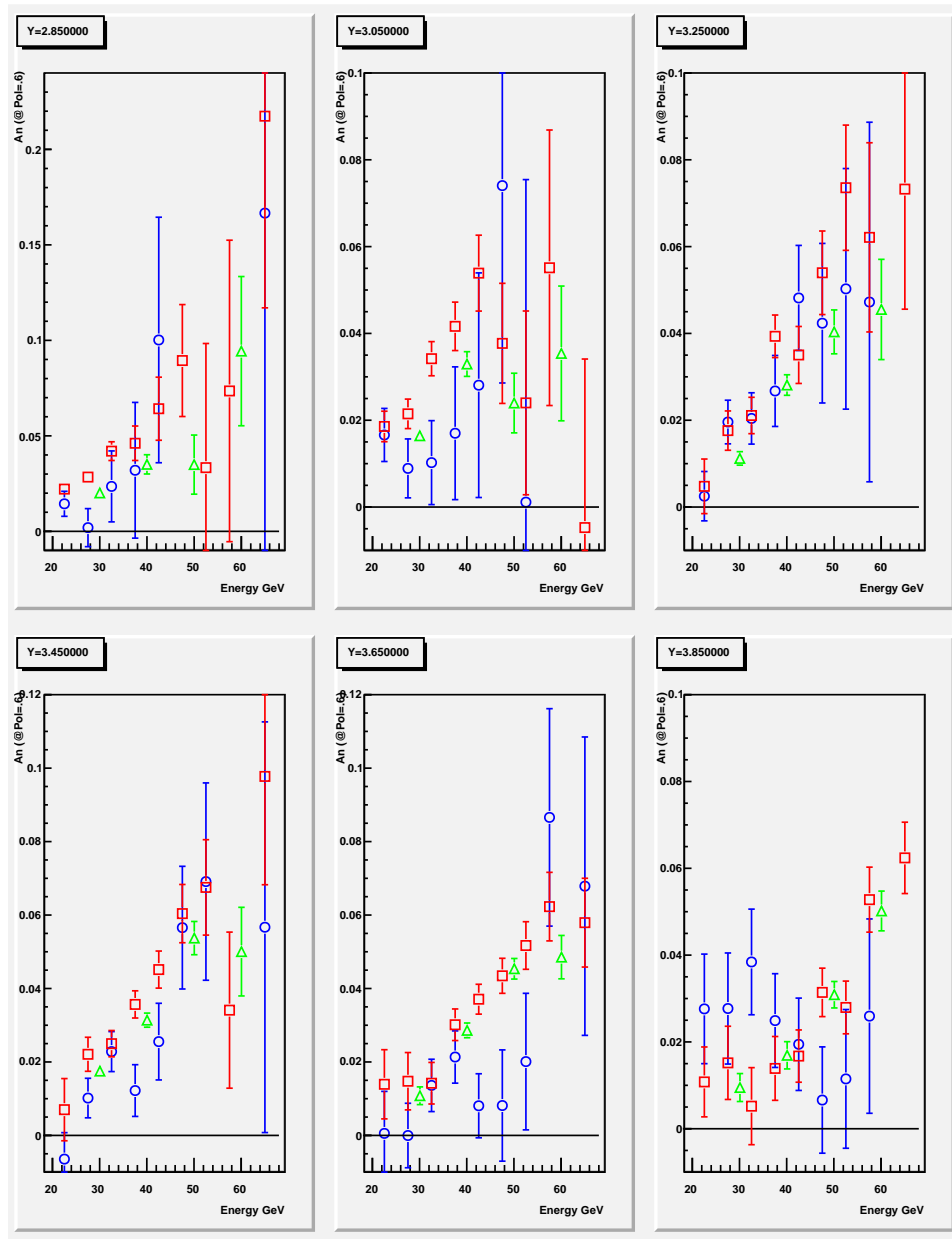


Figure 20: This figure compares 3 classes of events. Red squares: 200mR; 2 photon; no soft energy. Green triangles: 35mR; 2 photons; soft energy. Blue circles: three photons in 35mR cone;  $\pi^0$  mass cut on high energy photon pair.

## Azimuthal Angular Dependence of Non-Cluster Photons (35mR 2 Photon Cluster)

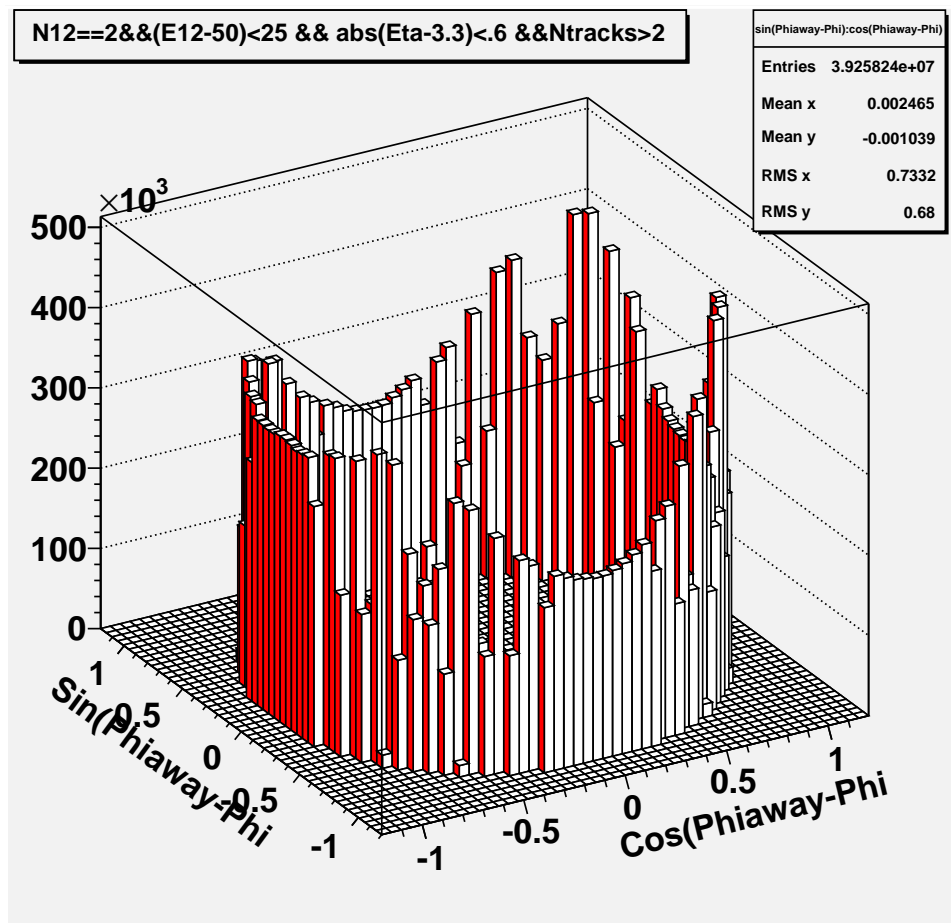


Figure 21: This plot displays the azimuthal angle dependence for 39 million 2 photon clusters with at least 1 additional photon. The angle plotted is  $(\phi_{away} - \phi)$  where  $\phi$  is the azimuthal angle of the 2 photon cluster and  $\phi_{away}$  is the azimuthal angle of the other photons in the event.

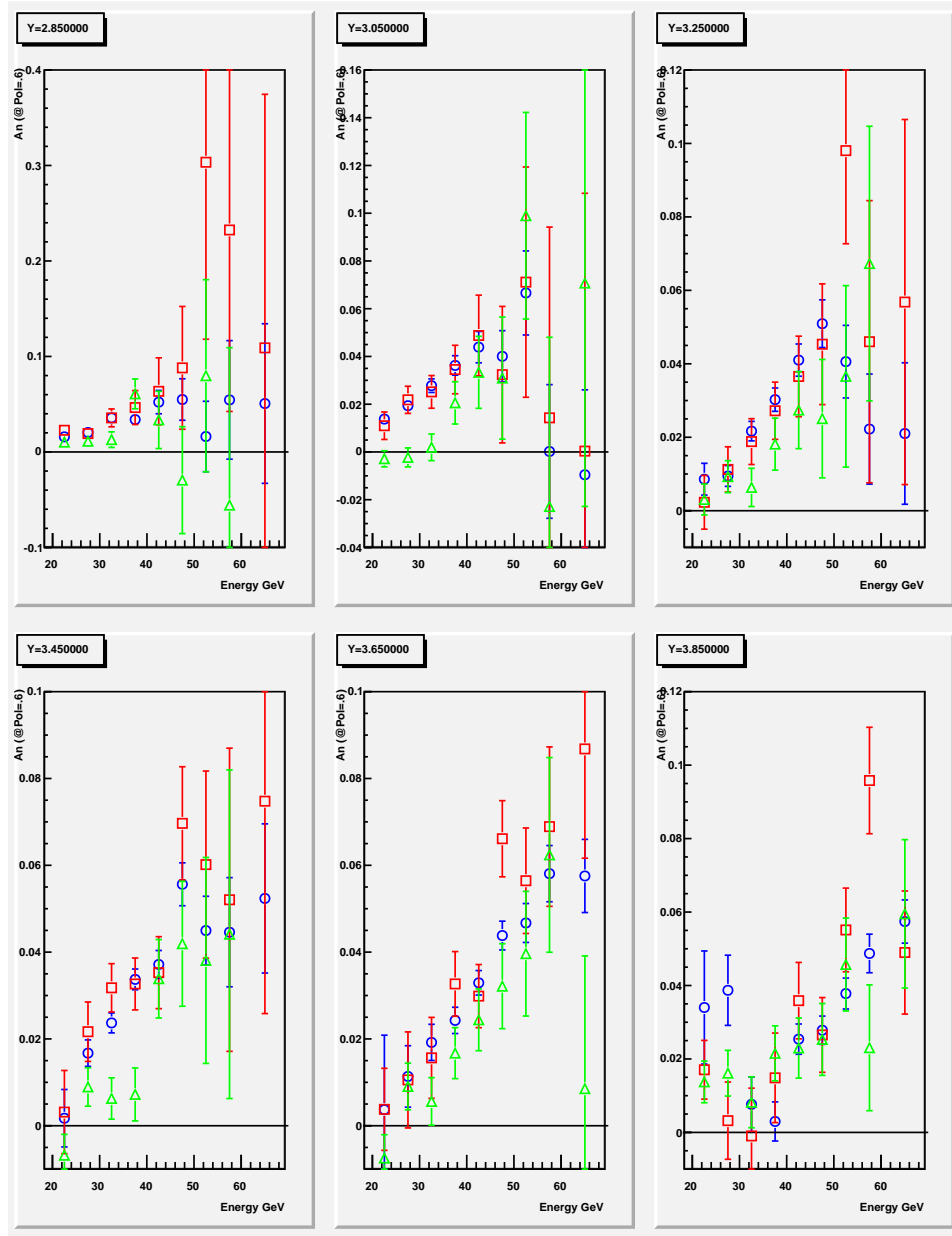


Figure 22: This plot compares three non-overlapping sets of events, all of which involve 2 photon clusters selected with the 35mR cone size. The 2 photons satisfy a mass cut  $|M_{12} - .135| < .08$ . Red squares: Additional photons, away from the cluster, have an azimuthal angle  $\cos(\phi_{away} - \phi) < -.5$ . Green triangles: Additional photons, away from the cluster, have azimuthal angle  $\cos(\phi_{away} - \phi) > 0$ . Blue circles: No additional photons.

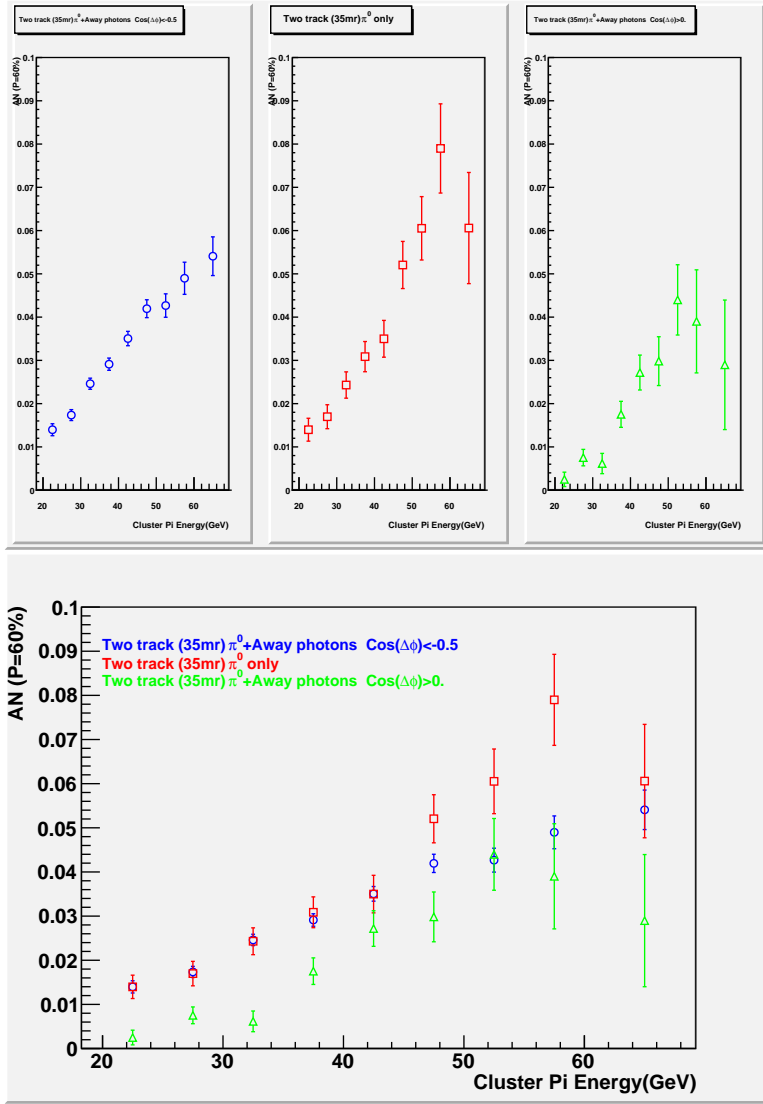


Figure 23: Top Frame: This plot compares three non-overlapping sets of events, all of which involve 2 photon clusters selected with the 35mR cone size. The plots show energy dependence for rapidity bins. The 2 photons satisfy a mass cut  $|M_{12} - .135| < .08$ . Red squares: Additional photons, away from the cluster, have an azimuthal angle  $\text{cos}(\phi_{\text{away}} - \phi) < -.5$ . Green triangles: Additional photons, away from the cluster, have azimuthal angle  $\text{cos}(\phi_{\text{away}} - \phi) > 0$ . Blue circles: No additional photons. Bottom Frame: Combination of the three plots from the top frame.

## Azimuthal Angular Dependence of $A_N$ for $\pi^0$ Pairs.

Here we consider 4 photon events with a two photon cluster of size 35mR with the two photon mass satisfying the  $\pi^0$  mass selection  $|M_{12}-0.135| < .08\text{GeV}$ . These events also contain a second photon pair that also satisfies the same mass selection cut. To avoid double counting, the energy of the second (Away side)  $\pi^0$  is less than the energy of the primary cluster  $\pi^0$ . Events are grouped according the azimuthal angle between the pair of  $\pi^0$ 's. Three groups are defined,

- Away side:  $\cos(\phi_{away} - \phi) < -0.5$
- Mid Azimuth:  $|\cos(\phi_{away} - \phi)| < 0.5$
- Near side:  $\cos(\phi_{away} - \phi) > 0.5$

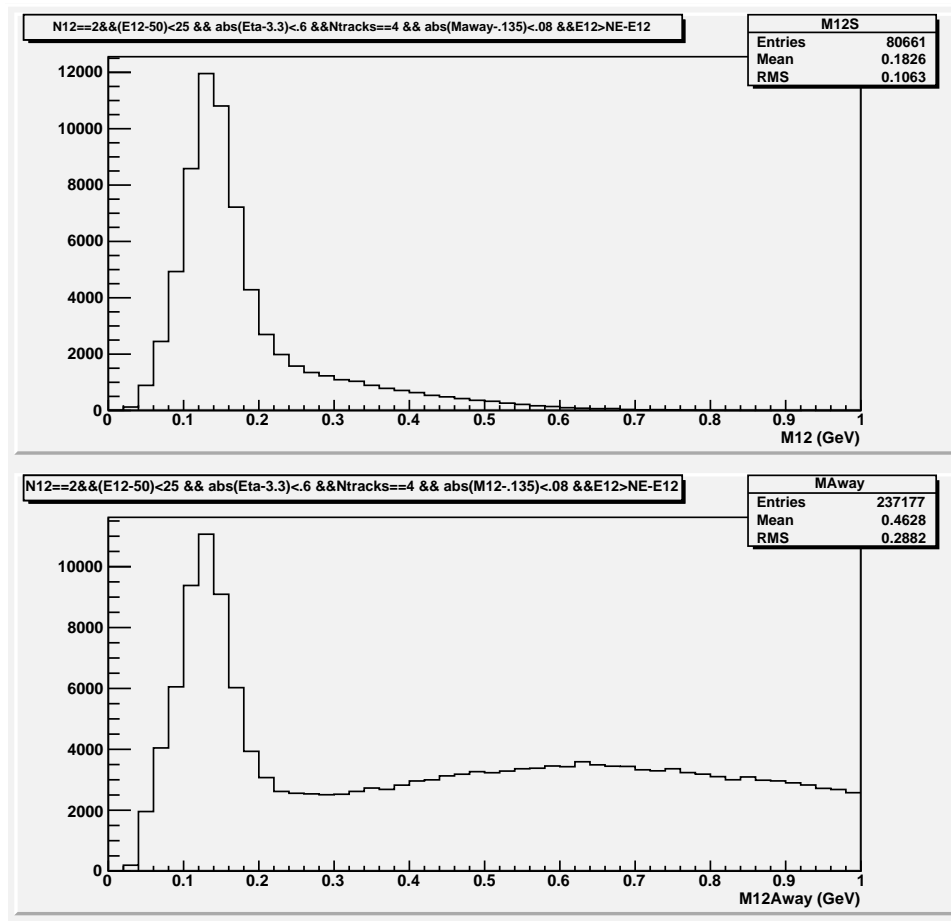


Figure 24: This plot shows top: Two photon cluster mass distribution when a second away side pair is found, with  $|M_{away} - 0.135| < .08$ . Bottom: The away side two photon mass distribution, with the same mass cut on cluster mass.



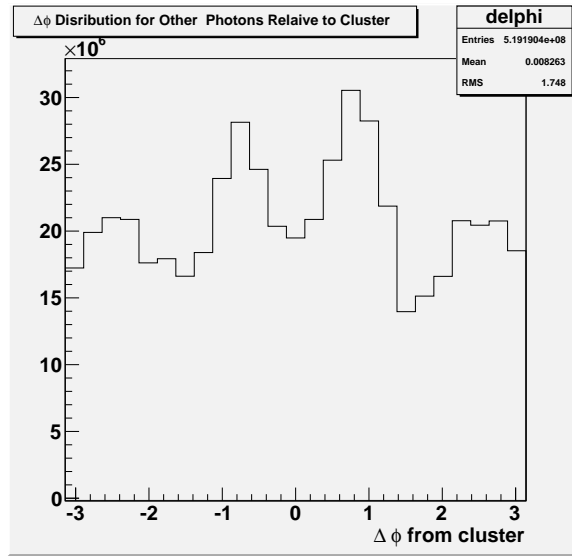


Figure 25: This plot shows the  $\Delta\phi$  distribution for all FMS analyzed events. One entry per cluster.

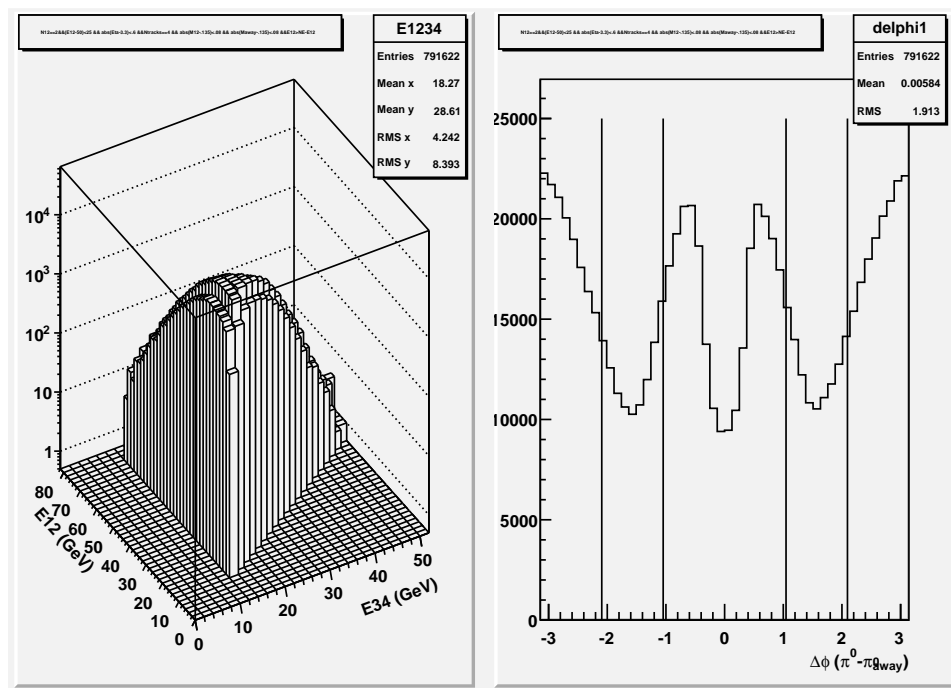


Figure 26: The plot on the left contains the energy distributions for pairs of  $\pi^0$ s. The first is selected with a cluster cone of  $35\text{mrad}$  and exactly 2 photons in the cluster. The event contains exactly 2 additional photons. The right plot displays the  $\Delta\phi$  distribution, the azimuthal distribution of the second  $\pi^0$  relative to the angle of the first. In both plots, both photon pairs are subjected to the mass cut  $|M - .135| < .08$  (GeV). The primary cluster  $\pi^0$  is in the energy range  $25 < E12 < 75$  GeV and the energy of the second photon is limited only by the low energy limit of each photon, (6 GeV). The pseudo-rapidity range is  $2.7 < Y < 3.9$ . There are about 80,000  $2 \pi^0$  pairs in this data sample.

The plots in Figure 27 show the energy dependence of asymmetry, averaged over the six pseudorapidity bins used above (full range 2.7-4.1). The horizontal axis corresponds to the energy of the cluster  $\pi^0$ .

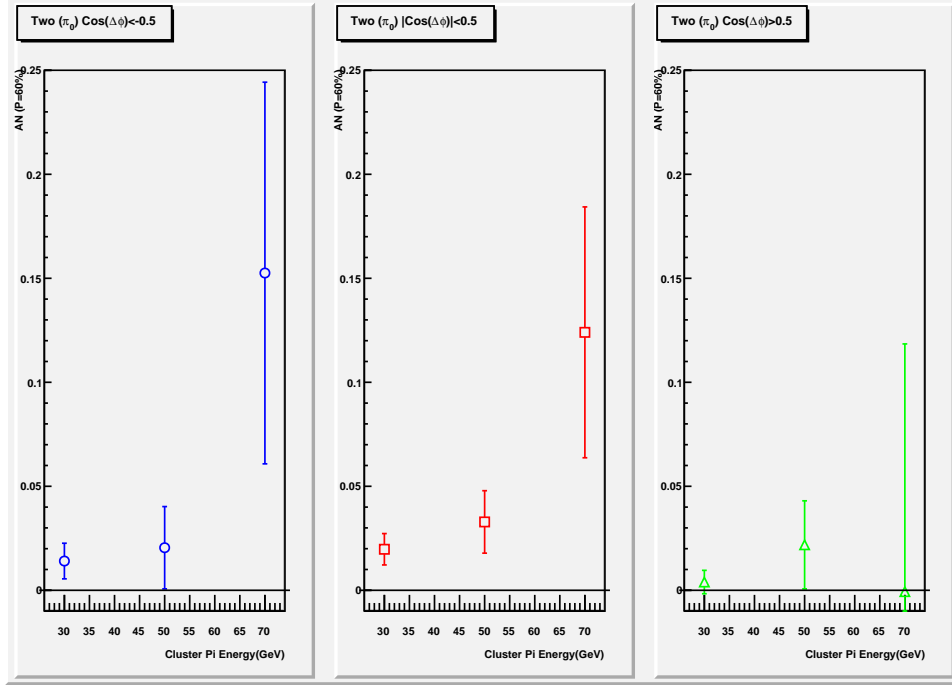


Figure 27: This plot shows the distribution of  $A_N$  (based on a primary two photon  $\pi^0$  cluster) as a function of the  $\pi^0$  cluster energy for events where there are two additional photons making a lower energy  $\pi^0$  outside the primary cluster. These plot compares three non-overlapping sets of events where in addition to the main  $\pi^0$  cluster (selected with the 35mR cone), with a two photon  $\pi^0$ . Both photon pairs satisfy the mass cut  $|M_{12} - .135| < .08$ . The horizontal axis represents the energy of the cluster  $\pi^0$  and  $A_N$  is obtained from the slop of the plot of  $\frac{N_{up} - N_{dn}}{N_{up} + N_{dn}}$  vs.  $\cos(\phi)$ . The azimuthal angle  $\phi$  is the azimuthal angle of the cluster. The away side azimuthal angle is referred to as  $\phi_{away}$ . Blue circles: Azimuthal angle between  $\pi^0$ 's satisfying  $\cos(\phi_{away} - \phi) < -0.5$ . Red squares: Same but with azimuthal angle  $|\cos(\phi_{away} - \phi)| < 0.5$ . Green triangles:  $\cos(\phi_{away} - \phi) > 0.5$ . The Green/Red/Blue points correspond to the regions marked in Figure 26.

In Figure 28, we examine the effect of looking only at higher energy away side  $\pi^0$ 's (Away Energy  $> 20$  GeV). We see by comparison with the effect of this cut is to increase the nominal value of  $A_N$  at the highest energy bin from the 10 to 15% range when  $E_{away} > 12$  GeV to the 20 to 25 % range for

$E_{away} > 20$  GeV, although these points are only 1 to 2 standard deviations from zero.

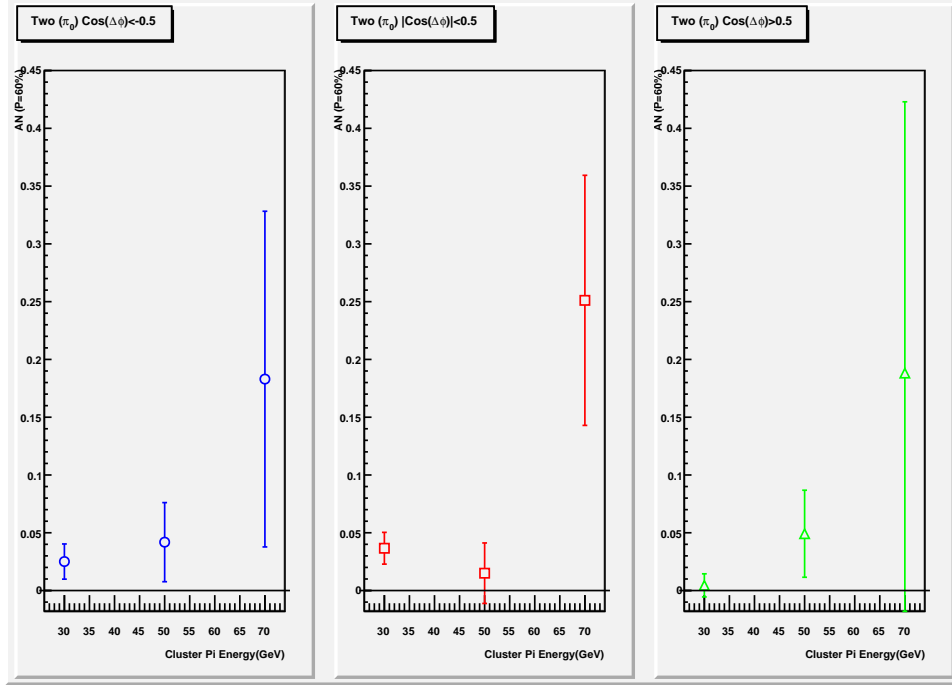


Figure 28: This plot shows the basic distribution of  $A_N$  seen in Figure 27 but with a more restricted energy requirement on the away side  $\pi^0$ . The additional selection is  $E_{away} > 20$  GeV. Left to right, the figures correspond to  $\cos(\phi_{away} - \phi) < -0.5$ ,  $|\cos(\phi_{away} - \phi)| < 0.5$  and  $\cos(\phi_{away} - \phi) > 0.5$ .

### $A_N$ vs Energy Sum of $\pi^0$ Pair.

Another approach is to plot the dependence of  $A_N$  vs. two  $\pi^0$  energy for events with 2  $\pi^0$ s. In this case, we increase the statistics by lowering the required energy threshold for the softer  $\pi^0$  and increase the width of the  $\pi^0$  mass selection criterion,  $E_{away} > 16$  and  $|M_{12} - .135| < .12$  and  $|M_{away} - .135| < .12$  (units GeV).

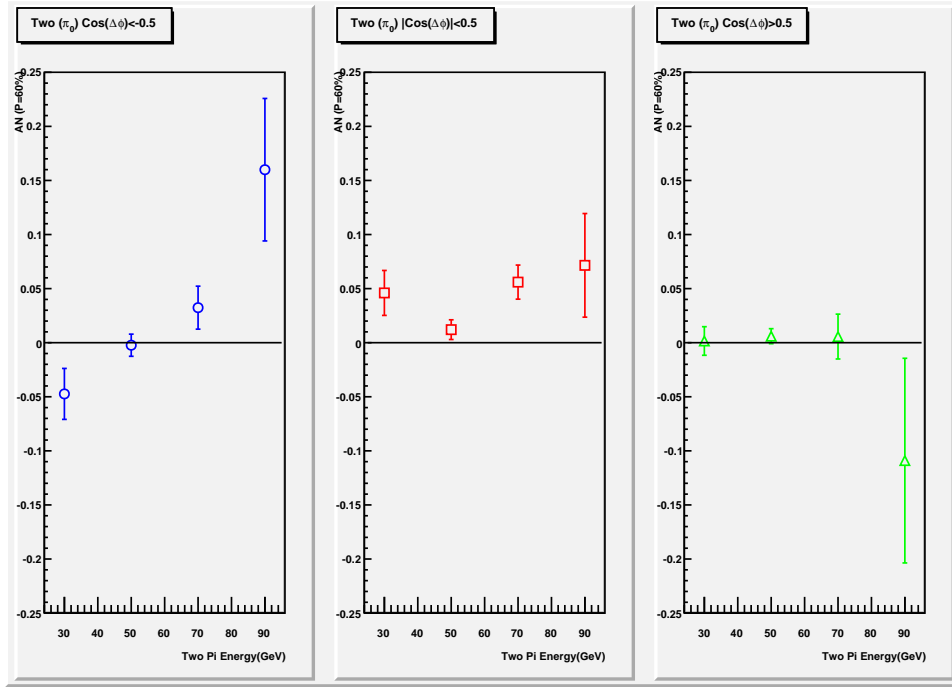


Figure 29: The distribution of  $A_N$  vs.  $E_{total}$  (the full event energy) for events with two  $\pi^0$ s. The primary cluster is selected with a 35mR cone angle. The masses are selected for  $E_{away} > 16$  and  $|M_{12} - .135| < .12$  and  $|M_{away} - .135| < .12$  (units GeV). Other cuts are the same as the previous figures (like Figure 28). Left to right, the figures correspond to  $\cos(\phi_{away} - \phi) < -.5$ ,  $|\cos(\phi_{away} - \phi)| < .5$  and  $\cos(\phi_{away} - \phi) > 0.5$ .

## Part V

### $A_N$ vs Transverse Momentum

In this section I show the dependence of  $A_N$  on transverse momentum ( $p_T$ ). Two photon clusters will be selected with a 35mR cone. The two photon mass is selected to be  $|M_{12} - 0.135| < .12$  GeV. Other cuts are  $z < 0.7$  and  $E_{soft} < 0.5$  GeV.

We see that the asymmetry increases with transverse momentum.

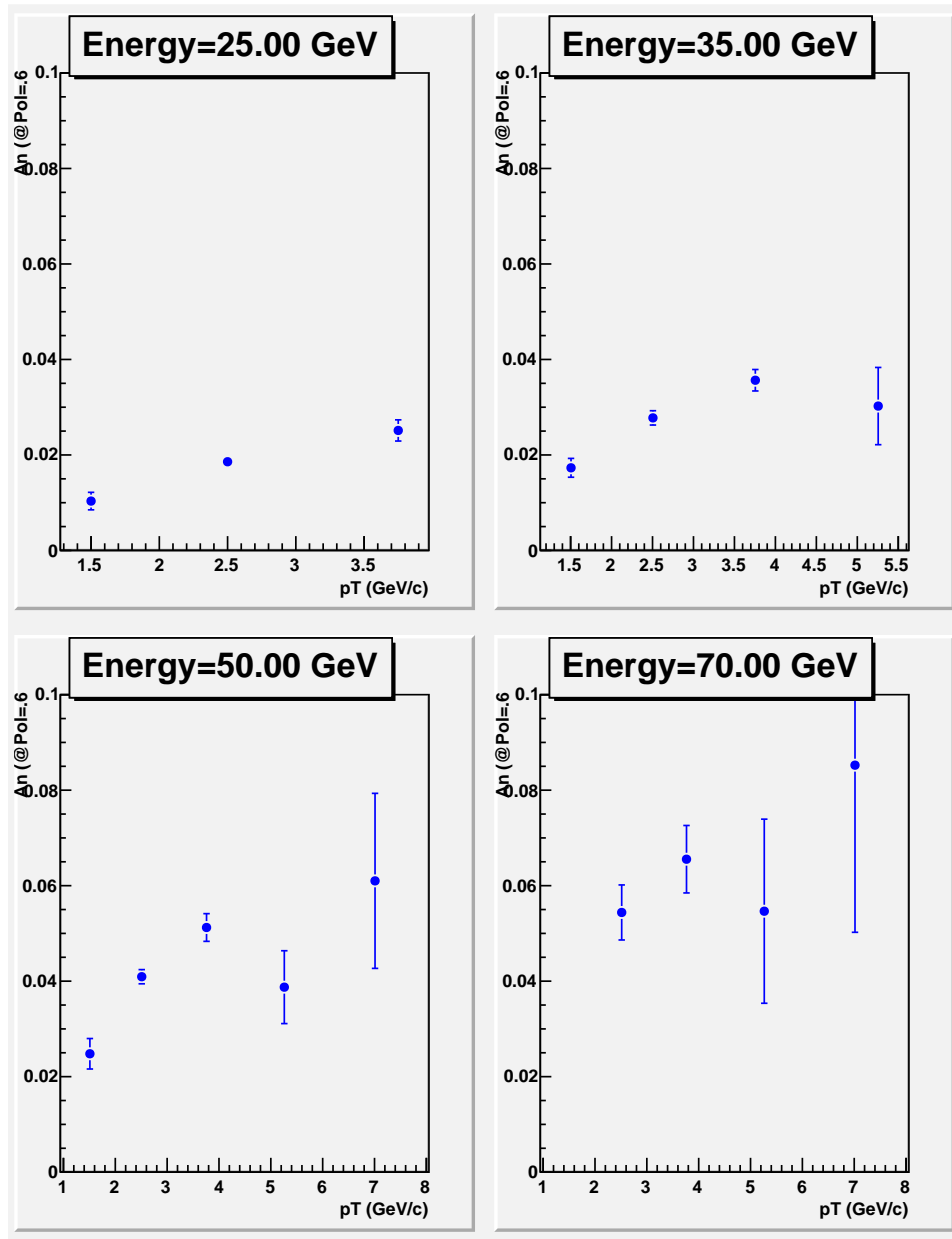


Figure 30: The distribution of  $A_N$  vs.  $p_T$  for 35 mR two photon clusters. The two photon mass is selected to be  $|M_{12} - 0.135| < .12$  GeV. Other cuts are  $z < 0.7$  and  $E_{soft} < 0.5$  GeV.



## Compare 200GeV and 500 GeV Dependence on $p_T$ .

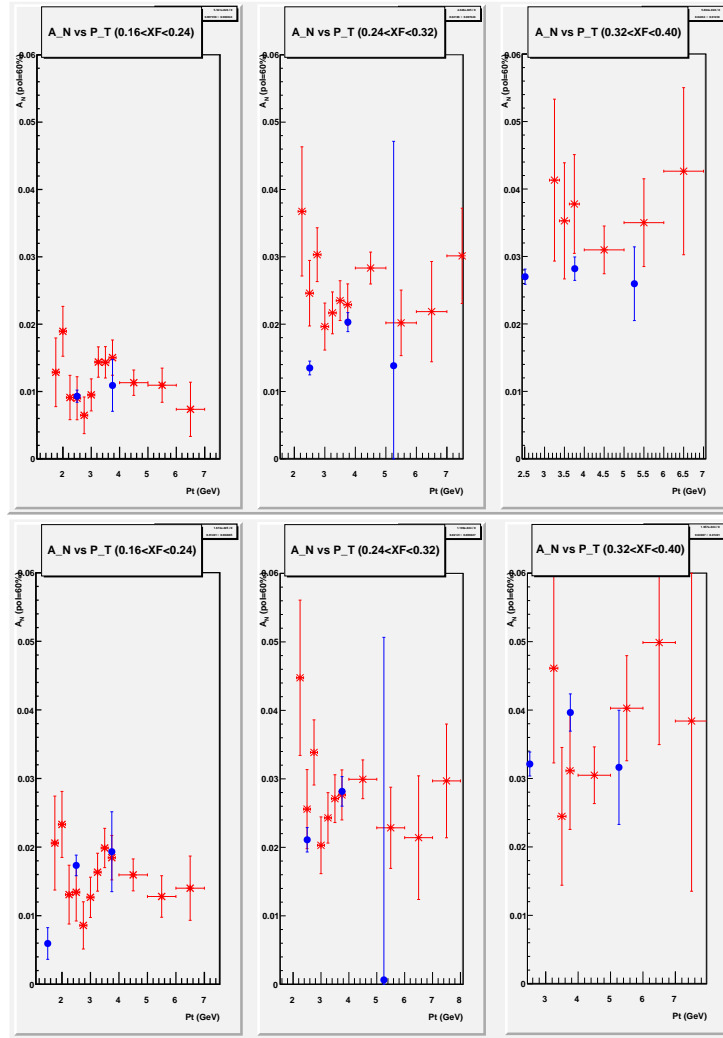


Figure 31: The distribution of  $A_N$  vs.  $p_T$ , comparing different center of mass energy for the same  $X_F$ . 200 GeV (blue circles) and 500 GeV (red stars) Two photon clusters selected with 30 or 35 mR (Top) and 70 mR (bottom) cluster angles. The 30 mR cluster was used at 500 GeV. The 200 GeV two photon mass is selected to be  $|M_{12} - 0.135| < .12$  GeV. The other cut is  $z < 0.7$ . From left to right, the  $X_F$  ranges are (.16-.24), (.24,.32) and (.32,.40).